Bol. Soc. Paran. Mat.
©SPM – E-ISSN-2175-1188
SPM: www.spm.uem.br/bspm

(3s.) **v. 2026 (44) 9** : 1–23.
ISSN-0037-8712
doi:10.5269/bspm.79337

Vaccination and Covering Behaviors Against Mpox: Timing, Effectiveness and Robustness

Shilpi Jain, Taye Samuel Faniran, Matthew O. Adewole, L. N. Nkamba, Praveen Agarwal and Hossein Jafari

ABSTRACT: When it comes to the control of mpox, vaccination plays a key role, but there are supply and uptake limiations faced by real world rollout. Lesion covering is a simple, low-cost behavior that could reduce transmission immediately, yet its role has remained underexplored. This study presents a modeling framework that incorporates vaccination throughput, vaccine efficacy, adoption of covering, protection durability, and persistence. Using this framework, we simulated U.S. outbreak patterns under vaccination-only, covering-only, and combined approaches. We assessed the consistency of outcomes across uncertain parameters through global sensitivity analysis and Latin Hypercube sampling. We show that vaccination and covering are not substitutes but synergistic levers. Vaccination alone reduces cumulative cases by 34.2% and yields epidemic control in only 24.3% of simulations. Covering alone contributes almost nothing (-0.2%; 0% chance of control). In contrast, combining both cuts cumulative burden by 80.0% and nearly doubles the probability of suppression ($P(R_e < 1)$ rises from 0.243 to 0.476). Persistence matters: when covering rapidly wanes, its impact disappears, but when sustained, it markedly enhances vaccination effectiveness. Global sensitivity analyses reveal four dominant drivers; transmission, recovery, covering protection, and two-dose effectiveness, with behavioral reversion strongly shaping outcomes. Our results demonstrate that lesion covering is best understood not as a standalone solution, but as a force multiplier for vaccination. By extending coverage before vaccines reach scale and by sustaining reductions afterward, covering nearly doubles the likelihood of epidemic control.

Keywords: Mpox, epidemic modeling, vaccination, lesion covering, outbreak control.

Contents

2020 *Mathematics Subject Classification:* 92D30, 92D25.
Submitted October 04, 2025. Published June 03, 2026.

1. Introduction

Since the start of the 2022 global outbreak caused by clade IIb mpox, more than 124,753 cases and over 272 deaths have been reported across 128 countries. According to the US CDC and WHO, the United States has documented 34,490 cases as of December 31 2024, with the pace of domestic transmission slowing in late 2024 and early 2025 [10]. While the number of reported cases has fallen since the height of mid-2022, low-level transmission persists; by September 1, 2024, U.S. CDC data documented 1,968 nationwide cases of clade II mpox nationwide, reflecting ongoing transmission [20]. At the same time, simple preventive actions, such as covering visible lesions, can reduce the likelihood of infectious contact. However, uptake of these measures within affected communities has been uneven, and their effectiveness under real-world conditions remains uncertain effectiveness remains uncertain. Current evidence syntheses emphasize that avoiding direct contact, covering lesions, and wearing a medical mask can reduce onward transmission, but no trials have directly quantified the magnitude of this effect [16]. These factors together leave public health agencies without clear quantitative guidance on how vaccination and covering behaviors interact to shape epidemic outcomes, or which mix of interventions can most effectively suppress transmission under real-world constraints.

Mathematical models of mpox transmission have so far focused primarily on vaccination. Studies have examined vaccine effectiveness, projected coverage requirements for epidemic control, and assessed delays in rollout, consistently showing that high and sustained vaccination is needed to drive the effective reproduction number below one. Yet behavioral mitigation measures such as lesion covering have received far less attention, often treated as marginal or neglected entirely. This omission is important. The effect of lesion covering on disease spread is determined by three main uncertainties: the share of individuals who adopt it (adoption rate), the extent to which it blocks infectious contact once implemented (protection strength), and the length of time it is maintained before waning due to factors such as fatigue or stigma (persistence). These behavioral elements can strongly shape epidemic dynamics, yet their quantitative impact remains poorly defined in current modeling work.

Mathematical modeling efforts on mpox have advanced rapidly in recent years, but with a nearly exclusive focus on vaccination. For example, Batiha et al. [5] formulated a fractional-order model of mpox transmission to capture memory effects in disease progression, while Mathivanan et al. [22], Kubra et al. [17], Agbata et al. [2], Ramzan et al. [26], Venkatesh et al. [30], and Addai et al. [1] extended this framework to incorporate Caputo-Fabrizio derivatives for improved realism in human-to-human spread. Research on mpox modelling that incorporates optimal control theory includes analyses conducted by Rashid et al. [27], De Jong et al. [12], Naandam et al. [24], and Rizk et al. [28] who estimated vaccination and treatment as possible intervention strategies. In complementary studies, Paparini et al. [25] and Jin et al. [15] evaluated the effects of quarantine and isolation, while Elemuwa et al. [13] and Shen et al. [29] analyzed approaches for optimizing resource distribution. Simulation approaches based on agent and network structures have been applied to forecast outbreak patterns under different levels of vaccine coverage, showing that both rapid deployment and high uptake are critical for effective control. [6,21,3]. From an economic perspective, analyses by: Idisi et al. [14,19,31,4] have evaluated the cost-effectiveness of targeted vaccination programs in settings with limited resources. However, none of these efforts explicitly represent lesion covering as a separate epidemiological state with its own adoption, protection strength, and persistence parameters, despite public guidance recommending covering lesions to reduce infectiousness [16]. Nor do they test how covering interacts quantitatively with vaccination rollout and behavioral persistence under uncertainty. Collectively, these studies show the progress made in modeling vaccination but also point out the vital need to broaden the scope to include behavioral interventions such as lesion covering.

To address this gap, we develop a quantitative modeling framework that addresses the question of how vaccination throughput and lesion-covering behaviors interact to determine mpox control. Our research question is: What mix and timing of vaccination and covering most effectively reduce transmission and burden in the United States, and how robust are these gains to uncertainty? Our investigation is organized around six main objectives that guide the analysis. First, we evaluate how adoption, protection strength, and persistence of covering reshape epidemic trajectories. Second, we determine whether covering alone can bend the epidemic curve before vaccination scale-up. Third, we quantify the relative contributions of vaccination and covering, as well as their interaction. Fourth, we assess the additional advantage gained

by integrating multiple intervention approaches. Fifth, we identify the biological and behavioral factors that most strongly shape the projected results. Finally, we examine whether our conclusions hold when subjected to broad, system-wide uncertainty.

2. Methods

2.1. Model Formulation

We develop a deterministic compartmental model to capture the transmission dynamics of Clade II Mpox in the United States (see Fig. 1). The total population $N(t)$ is divided into the following mutually exclusive epidemiological compartments: susceptible individuals $S(t)$, exposed (infected but not yet infectious) individuals $E(t)$, uncovered infectious individuals $I(t)$, covered infectious individuals $C(t)$, recovered individuals with immunity $R(t)$, individuals vaccinated with one dose $V_1(t)$, and individuals vaccinated with two doses $V_2(t)$. Thus,

$$N(t) = S(t) + E(t) + I(t) + C(t) + R(t) + V_1(t) + V_2(t).$$

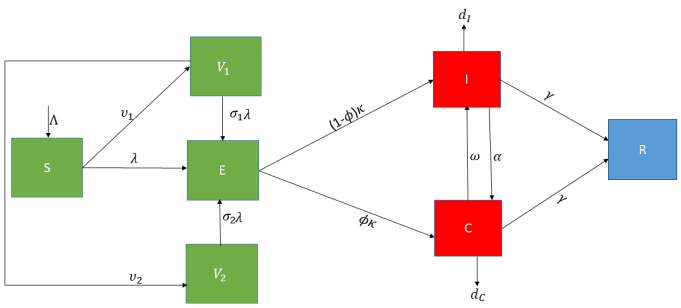

Figure 1: Transmission flow diagram of the Clade II Mpox model.

Model Description

Susceptible individuals S enter the population at rate Λ and may leave due to natural mortality at per-capita rate μ. The baseline transmission rate is denoted by β. The force of infection accounts for contributions from both uncovered infectious individuals I and covered infectious individuals C, the latter transmitting at a reduced level.

After an average latent period of $1/\kappa$ days, exposed individuals E progress to the infectious stage. A fraction ϕ of them adopt covering immediately and move into C, while the remainder enter I. Symptomatic infectious individuals in I may also transition into the covered class C at rate α, reflecting adoption of lesion covering or reduction in risky contacts, whereas individuals in C may abandon covering and revert to I at rate ω.

Individuals in C remain symptomatic but transmit at reduced intensity. Specifically, covering lesions or reducing close contacts diminishes onward transmission [11]. We let $\rho \in (0, 1)$ denote the fractional reduction in per-contact transmissibility, and $\theta \in (0, 1)$ the fractional reduction in effective contact rates. Their product

$$r = \rho\theta$$

represents the overall proportional reduction in transmission relative to uncovered infectious individuals. Both I and C recover at rate γ and move into R, which confers immunity. There are disease induced death rates of d_I and d_C. There are residual susceptibility and 1 dose and after 2 doses at rates σ_1 and σ_2 [8]. There are also first and second time dose at rates ν_1 and ν_2.

Vaccination reduces susceptibility only. Individuals can receive one or two doses of vaccine. One dose reduces risk by a factor $\sigma_1 \in (0, 1)$, while two doses confer higher protection $\sigma_2 \in (0, 1)$, with $\sigma_2 \ll \sigma_1$ [8]. Vaccinated individuals remain in their classes but may still experience breakthrough infection at the reduced probabilities σ_1 and σ_2, respectively.

2.2. Model Equations

The force of infection is given by

$$\lambda(t) = \frac{\beta}{N(t)}\big(I(t) + (1-r)C(t)\big), \tag{2.1}$$

where β is the baseline transmission rate and r is the proportional reduction in transmissibility of covered infectious individuals.

The full SEIRV-C system of ordinary differential equations is:

$$\frac{dS}{dt} = \Lambda - \lambda S - \nu_1 S - \mu S, \tag{2.2}$$

$$\frac{dV_1}{dt} = \nu_1 S - \sigma_1 \lambda V_1 - \nu_2 V_1 - \mu V_1, \tag{2.3}$$

$$\frac{dV_2}{dt} = \nu_2 V_1 - \sigma_2 \lambda V_2 - \mu V_2, \tag{2.4}$$

$$\frac{dE}{dt} = \lambda S + \sigma_1 \lambda V_1 + \sigma_2 \lambda V_2 - (\kappa + \mu)E, \tag{2.5}$$

$$\frac{dI}{dt} = (1-\phi)\kappa E + \omega C - (\alpha + \gamma + \mu + d_I)I, \tag{2.6}$$

$$\frac{dC}{dt} = \phi\kappa E + \alpha I - (\omega + \gamma + \mu + d_C)C, \tag{2.7}$$

$$\frac{dR}{dt} = \gamma I + \gamma C - \mu R. \tag{2.8}$$

2.3. Disease-Free Equilibrium and Effective Reproduction Number R_e

We consider the full SEIRV–C system (vaccination allowed). At DFE,

$$E^* = I^* = C^* = R^* = 0, \qquad \lambda^* = 0.$$

Demography–vaccination balance (with recruitment Λ and natural mortality μ) gives

$$S^* = \frac{\Lambda}{\nu_1 + \mu}, \qquad V_1^* = \frac{\nu_1}{\nu_2 + \mu}\, S^*, \qquad V_2^* = \frac{\nu_2}{\mu}\, V_1^*, \qquad N^* = S^* + V_1^* + V_2^*.$$

Define the effective susceptible load

$$S_{\text{eff}} \;\equiv\; S^* + \sigma_1 V_1^* + \sigma_2 V_2^*.$$

To compute the Jacobian matrices at the DFE (infected subsystem $x = (E, I, C)^\top$), let

$$b \;=\; \beta\, \frac{S_{\text{eff}}}{N^*}, \qquad P \;=\; \beta(1-r)\, \frac{S_{\text{eff}}}{N^*}.$$

Jacobians at the DFE are

$$F' \;=\; \begin{pmatrix} 0 & b & P \\ 0 & 0 & 0 \\ 0 & 0 & 0 \end{pmatrix}, \qquad V' \;=\; \begin{pmatrix} \kappa + \mu & 0 & 0 \\ -(1-\phi)\,\kappa & \alpha + \gamma + \mu + d_I & -\,\omega \\ -\,\phi\,\kappa & -\,\alpha & \omega + \gamma + \mu + d_C \end{pmatrix}.$$

To obtain the effective reproduction number, we write

$$\delta_I = \gamma + \mu + d_I, \qquad \delta_C = \gamma + \mu + d_C, \qquad D = (\alpha + \delta_I)(\omega + \delta_C) - \alpha\,\omega.$$

From the next-generation matrix $K = F'(V')^{-1}$, the spectral radius yields

$$R_e \;=\; \beta\, \frac{S_{\text{eff}}}{N^*}\, \frac{\kappa}{\kappa + \mu}\, \frac{\omega + (1-\phi)\,\delta_C \;+\; (1-r)\big(\alpha + \phi\,\delta_I\big)}{(\alpha + \delta_I)(\omega + \delta_C) - \alpha\,\omega}.$$

Setting $V_1^* = V_2^* = 0$ (so $S_{\text{eff}} = S^*$) recovers the basic reproduction number R_0 for the non-vaccinated system.

3. Model Fitting and Parameter Estimation

We calibrated the SEIRV-C system to the U.S. Clade II mpox epidemic by fitting the model to daily laboratory-confirmed cases reported by the U.S. Centers for Disease Control and Prevention (CDC) from March 2022 through March 2025 [7]. The CDC public portal (https://www.cdc.gov/mpox/) provides national time series updated monthly (we used the daily case counts to inform transmission and behavioral parameters). We minimized the sum of squared errors (SSE) between observed daily cases and the model-implied daily incidence. The ODEs were solved with a variable-step Runge-Kuta method (*ode*45). Parameters were estimated with nonlinear least squares lsqcurvefit under simple bounds to ensure biological plausibility. $R^2 = 0.9688$ showing that the model's prediction perfectly matched the observed data (Figure 2).

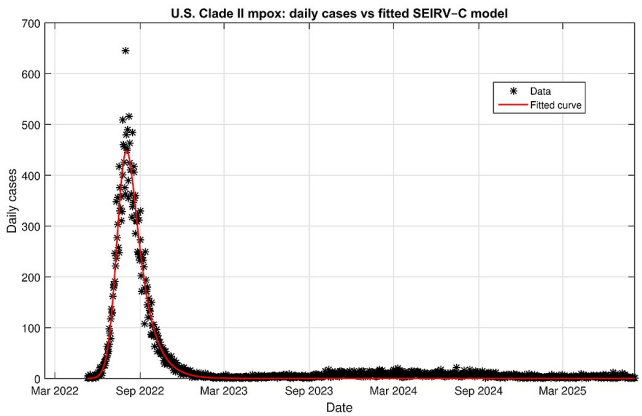

Figure 2: Model fitting on the observed data. Data source: CDC national mpox case trends, March 2022-March 2025 [7].

Table 1 lists all parameters, indicating which were fitted versus fixed from literature.

Table 1: Model parameters used in fitting the SEIRV-C model to U.S. Clade II mpox daily cases (March 2022-March 2025).

Parameter	Description	Value/Units	Reference
β	Rate of transmission	0.737 day^{-1}	fitting
r	Overall reduction in transmission for C	0.516 ($\approx$ 52% reduction)	fitting
α	Adoption rate of covering ($I \to C$)	0.213 day^{-1}	fitting
ω	Reversion rate ($C \to I$)	0.103 day^{-1}	fitting
γ	Recovery rate	0.0737 day^{-1}	fitting
κ	Progression rate $E \to I, C$	0.181 day^{-1}	fitting
ν_1	First dose vaccination rate	0.0228 day^{-1}	fitting
ν_2	Second dose vaccination rate	0.0500 day^{-1}	fitting
σ_1	Residual susceptibility after 1 dose	0.417	fitting
σ_2	Residual susceptibility after 2 doses	0.104	fitting
N_{pop}	Effective at-risk population size	227,959	fitting
μ	Natural mortality rate	3.54×10^{-5} day^{-1}	[8]
Λ	Recruitment rate	8.06 persons/day	derived from μN_{pop}
ϕ	Fraction of E progressing directly to C	0.6	Assumed
d_I, d_C	Disease-induced mortality rate for uncovered infectious	0.025	[23]
d_C	Disease-induced mortality rate for covered infectious	0.002	Assumed

4. Numerical Simulations and Results

4.1. Numerical Simulations

We performed numerical simulations of the model described in equations (2.2)–(2.8), using the fitted baseline parameter set in Table 1, to quantify how individual protective behaviors, lesion covering and reduced risky contacts, modulate population-level outcomes. Next, we analyze how adoption rate α, protection strength r, and reversion rate ω, affect the dynamics of epidemics over time. We then separated the individual contributions of vaccination and lesion covering, examined combined implementation schedules for both strategies (with the full optimal control model detailed in Appendix A), and performed robustness (through local and global sensitivity).

4.2. Impact of Adoption and Protection on Cumulative Infections

To assess how the uptake of protective behavior and its efficacy influence epidemic dynamics, we analyzed cumulative mpox infections across a three-year period (March 2022–March 2025, $\sim$ 1,100 days) across a two-dimensional parameter grid. The horizontal axis represents the protection factor r (the reduction in infectiousness conferred by adopting the covering behavior), while the vertical axis shows the adoption rate α (the per-capita rate at which infectious individuals adopt covering). For every (α, r) pairing, the heatmaps display cumulative infection totals, with color gradients and numeric labels indicating exact values and contour lines marking epidemiologically significant thresholds (25k, 50k, and 100k cases).

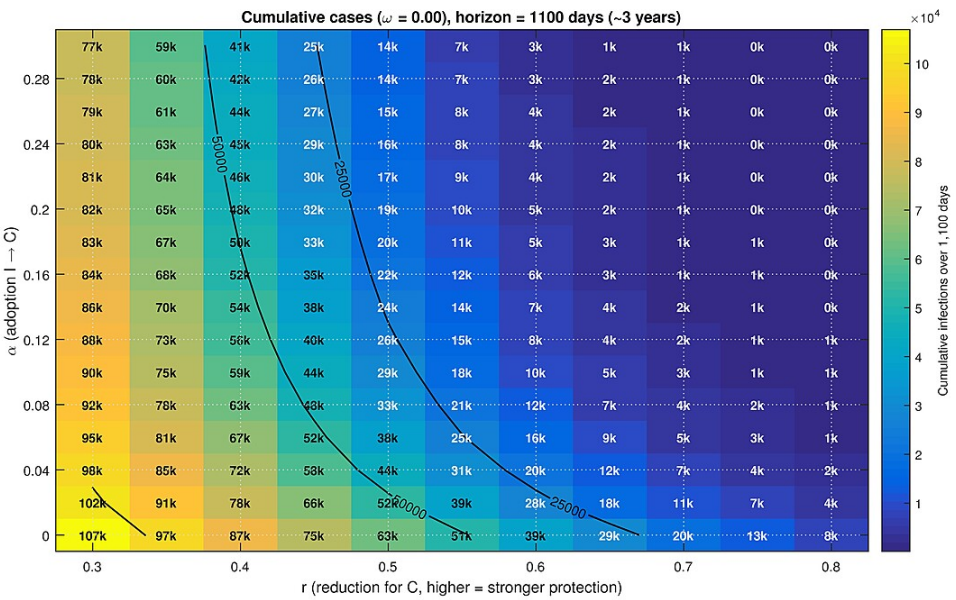

Figure 3: Cumulative mpox cases over March 2022–March 2025 ($\sim$ 1,100 days) as a function of adoption rate α and transmission reduction r under the baseline case of no reversion ($\omega = 0$). 25k, 50k, and 100k cases are the thresholds.

In Figure 3, perfect covering sustained with no reversion greatly reduces the epidemic. At low adoption ($\alpha < 0.05$) and weak protection ($r < 0.4$), cumulative infections exceed 100k. However, increasing either parameter yields pronounced reductions: for instance, moving from $r = 0.4$ to $r = 0.7$ at a modest adoption rate ($\alpha = 0.1$) reduces the total epidemic size from roughly 70k to below 20k. Significantly, combinations of high adoption ($\alpha > 0.2$) and strong reduction ($r > 0.7$) nearly eliminate epidemic spread, pushing cumulative cases close to zero. This shows a strong synergistic effect, where moderate improvements along both dimensions combine to generate disproportionately large reductions in total infections.

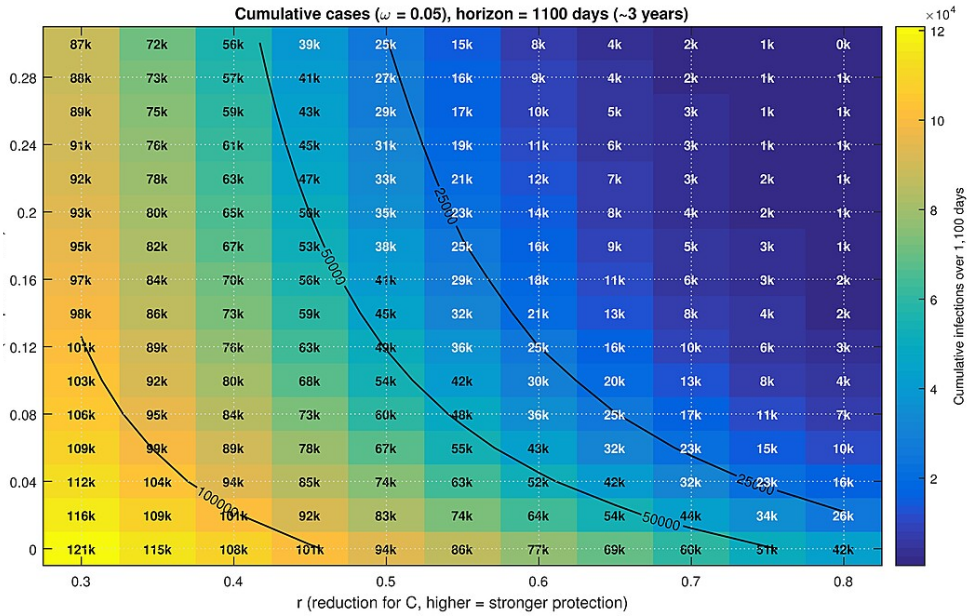

Figure 4: Same as Figure 3, but with moderate reversion ($\omega = 0.05$). Sustained protection is eroded, raising cumulative infections even at high adoption and strong reduction levels.

In Figure 4, allowing a modest reversion rate substantially erodes the benefits of adoption. Even with strong reduction $r = 0.7$, cumulative infections at $\alpha = 0.1$ now approach 30k, compared to less than 20k in the baseline case. The region where infections remain below the 25k contour shrinks considerably, requiring both high adoption and high reduction. In the figure, at $\alpha = 0.2$ and $r = 0.7$, total cumulative cases goes up to 11k, compared to when $\omega = 0$. This illustrates how even partial behavioral fatigue weakens the long-term impact of covering interventions.

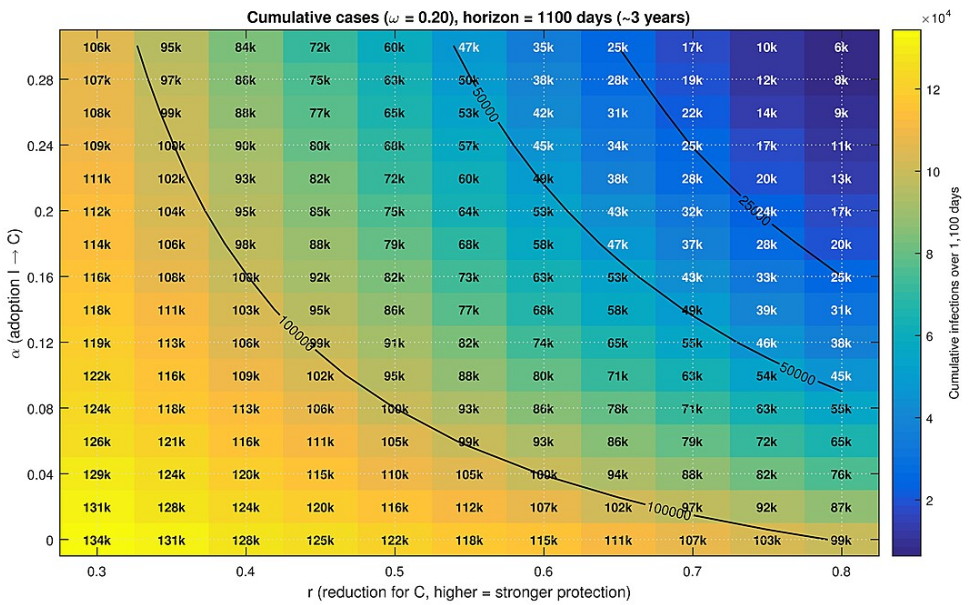

Figure 5: Same as Figure 3, but with high reversion ($\omega = 0.20$). Rapid abandonment of covering substantially reduces effectiveness of adoption, leaving high epidemic sizes even under favorable α and r.

In Figure 5, when reversion becomes rapid, the effectiveness of adoption collapses. Even under optimistic scenarios, high adoption ($\alpha > 0.2$) and strong reduction ($r = 0.7$), cumulative infections remain well above 50k, with many parameter combinations yielding epidemic sizes exceeding 100k. In this regime, contour lines become compressed, indicating that even large improvements in α or r are insufficient to offset rapid loss of protection. These results together reveal that behavioral protection is highly effective only if it is both strong (large r) and sustained (low ω).

4.3. Behavioral levers over time

To complement the heatmaps, we show full time trajectories of the exposed, infectious (uncovered), and covered classes $\big(E(t), I(t), C(t)\big)$ when we vary one behavioral parameter at a time and hold all others (including vaccination) at their fitted values.[1] Legends in each panel list the parameter values; the baseline curve is labeled *(baseline)*. Figure 6 plots $E(t), I(t), C(t)$ for several α values around the estimate.

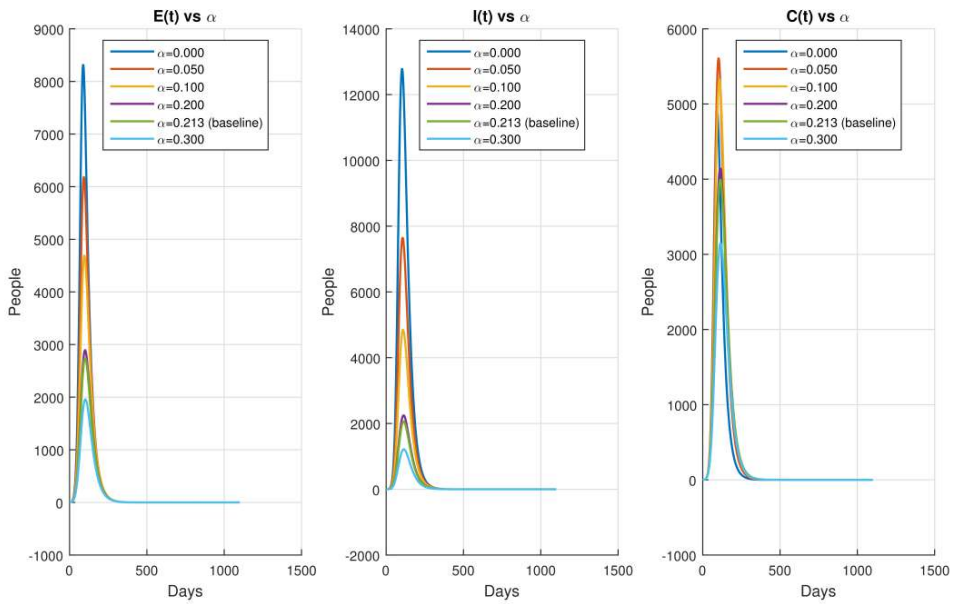

Figure 6: Time series with varying adoption rate α: trajectories of $E(t)$ (left), $I(t)$ (middle), and $C(t)$ (right). Vaccination and all other parameters are fixed at fitted values; the baseline $\alpha = 0.213$ is labeled. Increasing α lowers and advances the peaks of E and I, while C increases earlier but remains less transmissible by (2.1).

Figure 7 varies ω. Larger ω erodes the benefit of covering by cycling individuals back to the uncovered infectious state I, which pushes peaks upward across E, I, and C. small or zero ω implies sustained covering. This confirms that durability of protection is as important as adoption.

[1] Baseline (fitted): $\alpha = 0.213$, $r = 0.516$, $\omega = 0.103$; $\nu_1, \nu_2, \sigma_1, \sigma_2, \beta, \kappa, \gamma, \mu, \phi, d_I, d_C$ as in Table 1. The force of infection is given by (2.1) and the dynamics by (2.2)–(2.8).

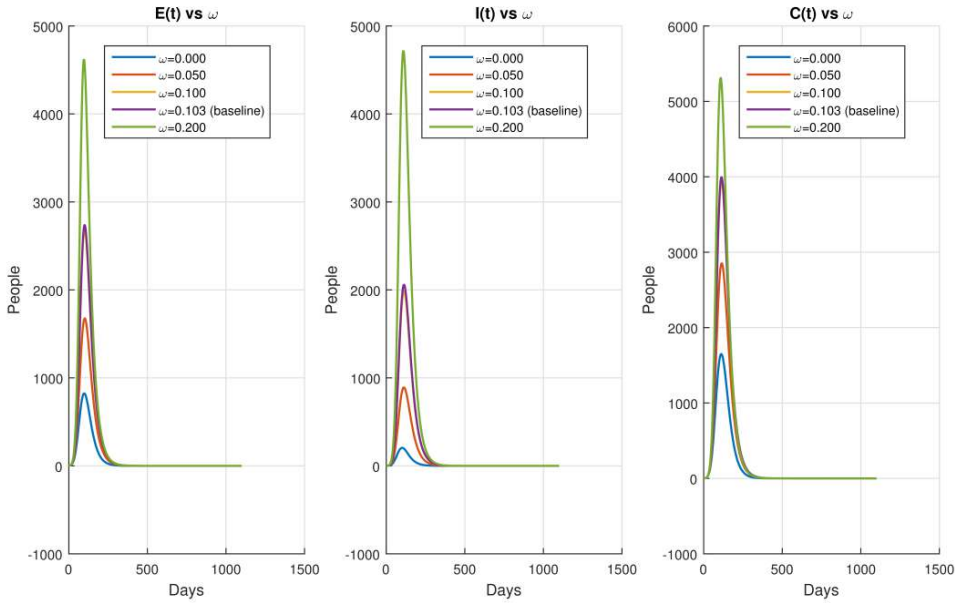

Figure 7: Higher ω (faster $C \to I$) weakens behavioral protection and raises peaks. With $\omega \approx 0$, covering persists and all peaks are substantially reduced.

Across all panels, the fitted baseline lies between curves in the expected order: higher adoption (α) and stronger reduction (r) reduce peaks and speed resolution; higher reversion (ω) does the opposite.

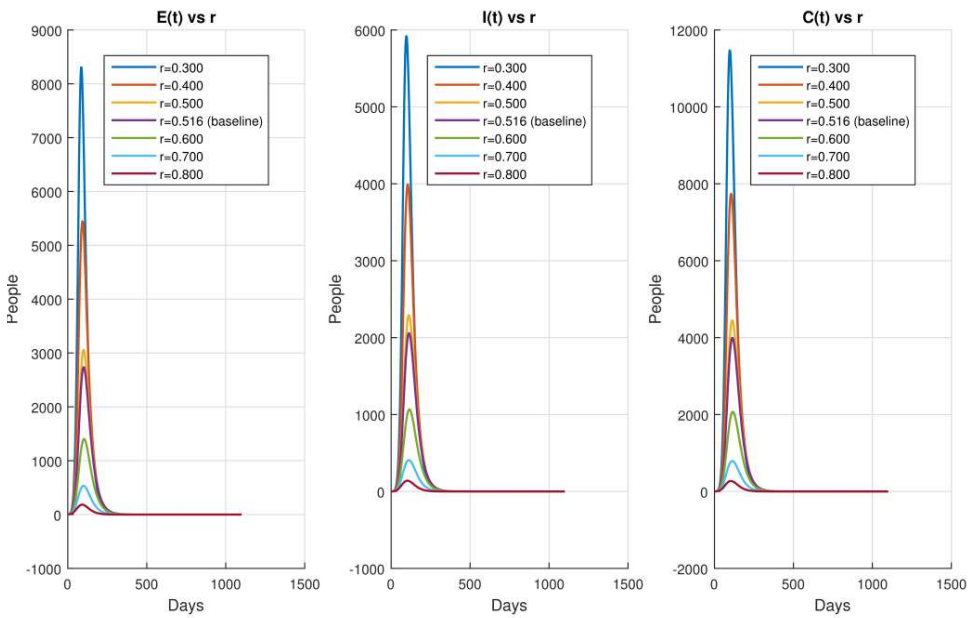

Figure 8: Time series with varying reduction r: $E(t)$, $I(t)$, $C(t)$. As r increases, the disease epidemic decreases

4.4. Relative Contributions of Vaccination and Lesion Covering

To disentangle the effects of vaccination and lesion covering, we ran four calibrated scenarios over the U.S. epidemic horizon (1,100 days): (i) None (no vaccination, no covering), (ii) Vaccination-only ($\nu_1, \nu_2, \sigma_1, \sigma_2$ at fitted values; $r = \alpha = 0$), (iii) Covering-only (r, α, ω at fitted values; $\nu_1 = \nu_2 = 0$), and (iv) Both (all fitted).

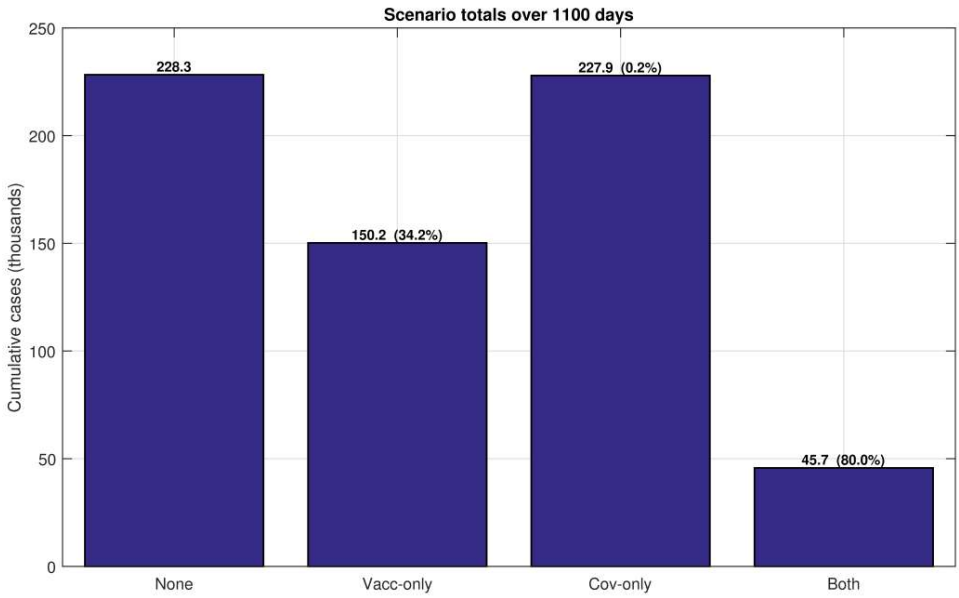

Figure 9: Total epidemic size under four counterfactuals.

Figure 9 establishes the baseline: the combination of vaccination and covering is dramatically more effective than either lever alone.

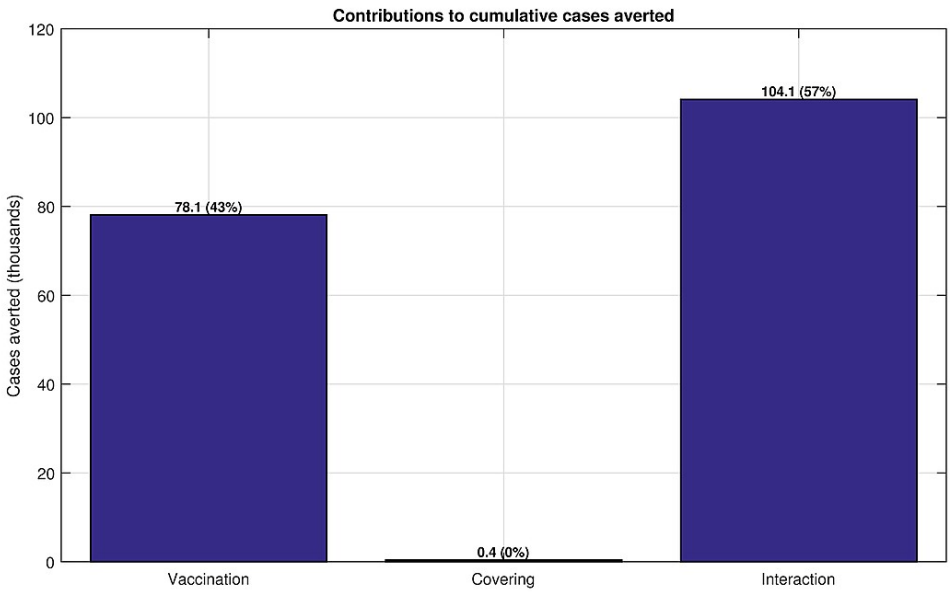

Figure 10: Attribution of cases averted.

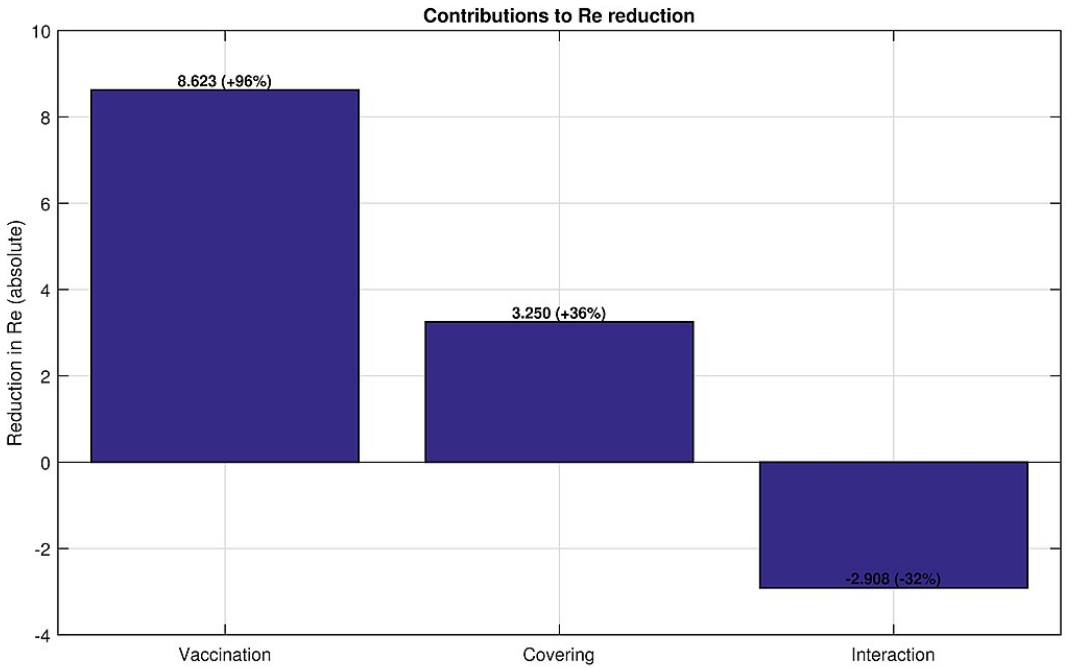

Figure 11: Attribution of the reduction in R_e at the DFE.

Vaccination emerges as the dominant independent driver of burden reduction under fitted U.S. parameters. While lesion covering alone yields modest effects at current adoption and efficacy levels, its value increases substantially when combined with vaccination: synergy between the two interventions accounts for approximately 57% of all cases averted.

4.5. Optimal Control Strategy

We evaluate policy schedules using the two practical levers introduced in the appendix: (i) vaccination intensity $u_v(t)$, which increases first- and second-dose throughput and reduces susceptibility, and (ii) covering reinforcement $u_c(t)$, which increases adoption/persistence of lesion covering and reduces effective infectiousness via the $I \leftrightarrow C$ pathway. The full optimal-control formulation (state equations with controls, objective functional, Hamiltonian, adjoints, and optimality conditions) is presented in Appendix A. Here we report implementation experiments that illustrate how u_v and u_c reshape the epidemic time paths for $E(t)$, $I(t)$, and $C(t)$ relative to the fitted baseline ($u_v \equiv 0$, $u_c \equiv 0$).

Figure 12 compares the reference trajectory (black) with the outcome under vaccination alone ($u_v > 0$, $u_c = 0$), and covering-only ($u_c > 0$, $u_v = 0$) trajectories. Both single levers visibly lower the epidemic peaks and accelerate decay across $E(t)$, $I(t)$, and $C(t)$.

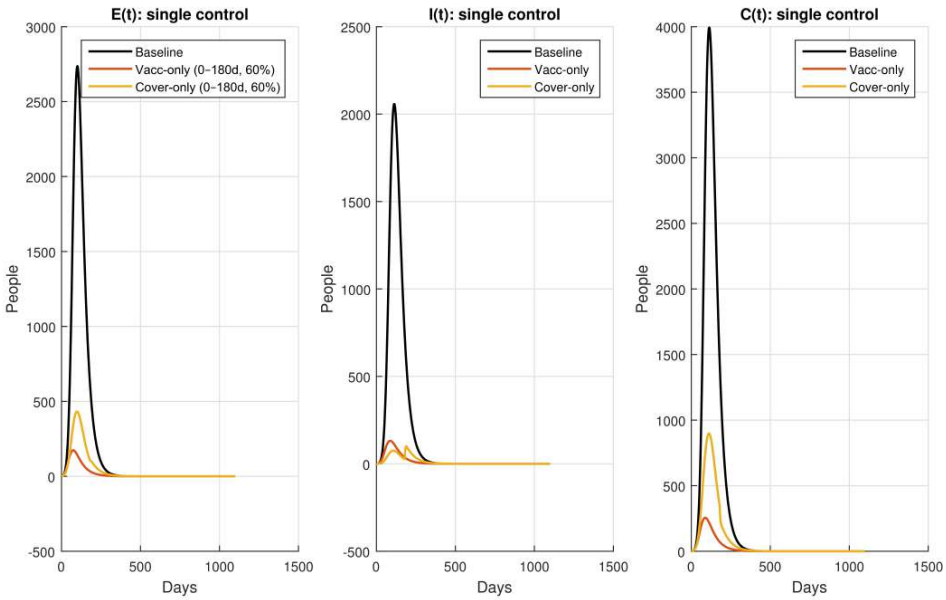

Figure 12: Single-control implementation. Baseline (black) vs vaccination-only (orange) and covering-only (gold) pulses $u_v(t) = 0.6$ or $u_c(t) = 0.6$ on days 0–180. Panels show $E(t)$, $I(t)$, $C(t)$.

Figure 13 adds the joint policy $u_v(t) = u_c(t) = 0.6$ for days 0–180. Combining levers yields the lowest peaks and quickest return to low prevalence among the "short, moderate" policies, reflecting complementarity between susceptibility reduction (vaccination) and infectiousness reduction (covering).

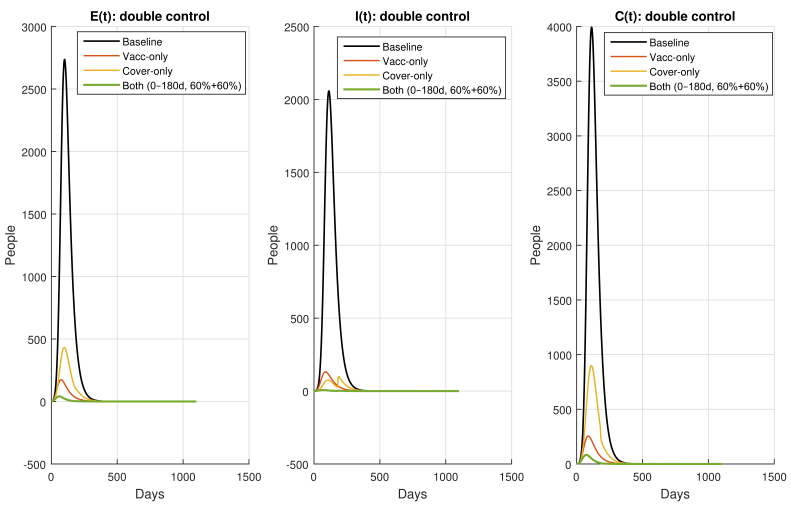

Figure 13: Double-control implementation (moderate, short). Baseline (black), each single control, and the joint policy $u_v = u_c = 0.6$ on days 0–180.

Figure 14 contrasts the moderate joint policy with a stronger, sustained campaign ($u_v(t) = u_c(t) = 1$ for days 0–365). With a longer window and full intensity, the epidemic is nearly flattened in all three compartments.

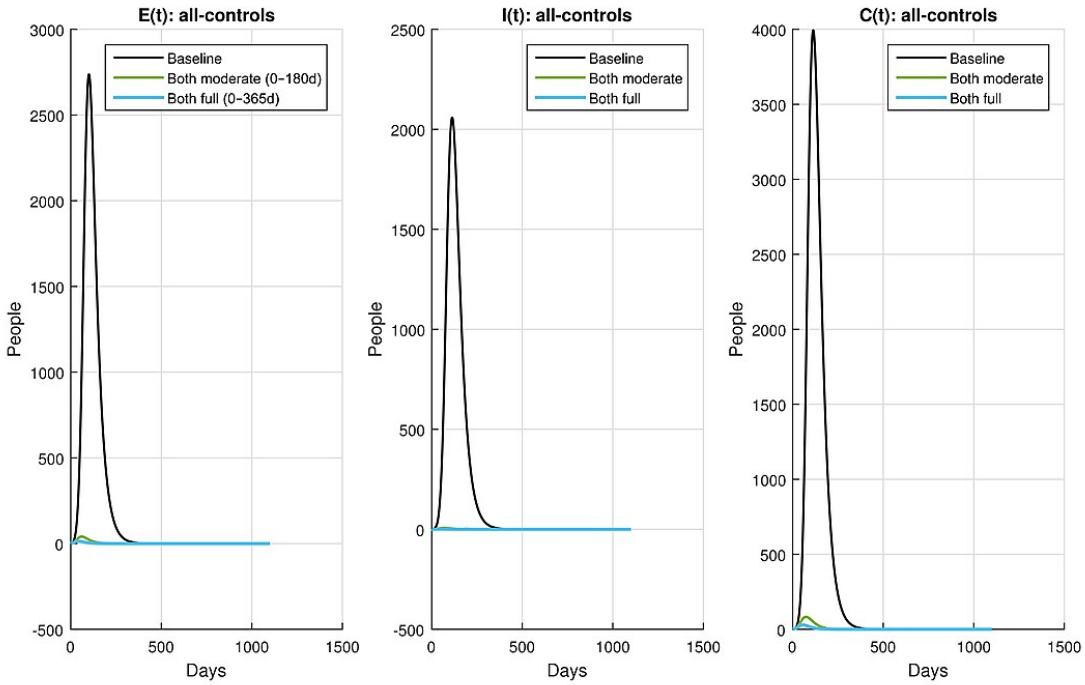

Figure 14: All-controls implementation (strong, sustained). Baseline (black), moderate joint policy (green, days 0–180), and full-year, full-intensity joint policy (blue, days 0–365).

4.6. Robustness and Local Sensitivity (One-at-a-Time Elasticities)

To assess robustness at the calibrated operating point (with both vaccination and covering active), we computed one-at-a-time (OAT) elasticities of two outcomes: (i) the effective reproduction number R_e at the DFE and (ii) 12-month cumulative cases, with respect to the model parameters $\{\beta, \kappa, \gamma, \nu_1, \nu_2, \sigma_1, \sigma_2, r, \alpha, \omega\}$. An elasticity $E_{Y,\theta}$ is interpreted as the percentage change in outcome Y per 1% change in parameter θ, evaluated at the fitted baseline (here approximated with a +5% finite difference). Positive values mean the outcome increases as the parameter increases; negative values mean the outcome decreases.

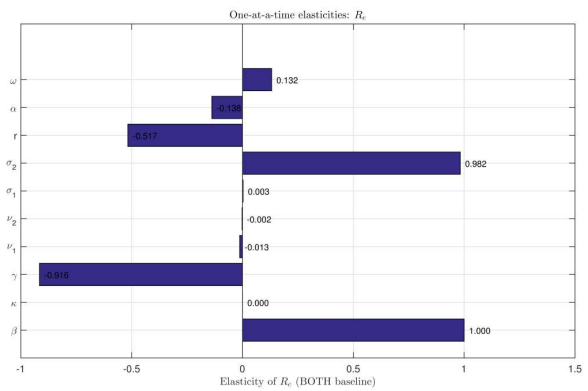

Figure 15: Local sensitivity of R_e (OAT elasticities). Bars show the percent change in R_e per 1% change in each parameter at the baseline with vaccination and covering active. The largest positive drivers of R_e are β and σ_2 (higher transmission or higher residual susceptibility after two doses), while γ (recovery), r (stronger reduction when covered), and, to a lesser extent, α (adoption) decrease R_e.

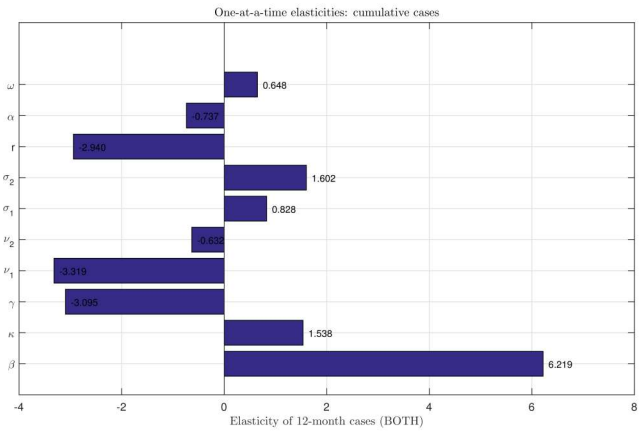

Figure 16: Local sensitivity of 12-month cumulative cases (OAT elasticities). Cumulative cases are most sensitive to β, with sizeable mitigating effects from γ, ν_1 (first-dose rate), and r. Parameters σ_1 and σ_2 (residual susceptibility after vaccination) increase cases; higher ω (reversion from covering) also increases cases.

Table 2 reports the elasticities that underlie Figs. 15–16. Three patterns stand out: (i) outcomes are highly sensitive to β; (ii) faster recovery (γ), faster first dosing (ν_1), and stronger covering efficacy (r) reduce both R_e and cases; (iii) Elevated residual susceptibility following the second vaccine dose (σ_2) significantly amplifies both R_e and case counts, showing the key role of strong two-dose vaccine efficacy.

Table 2: One-at-a-time elasticities at the "Both" baseline (finite-difference step +5%). Entries are $E = \frac{\Delta Y/Y}{\Delta\theta/\theta}$; positive (+) raises the outcome, negative (−) lowers it.

Parameter	$E[R_e]$	$E[\text{Cases}_{12\text{m}}]$
β	+1.000	+6.219
κ	+0.000	+1.538
γ	−0.916	−3.095
ν_1	−0.013	−3.319
ν_2	−0.002	−0.632
σ_1	+0.003	+0.828
σ_2	+0.982	+1.602
r	−0.517	−2.940
α	−0.138	−0.737
ω	+0.132	+0.648

These local sensitivities quantify where marginal changes "buy the most."

4.7. Global Sensitivity (GS) and Uncertainty (PRCC + LHS)

Here, LHS sample ($N = 1000$) is drawn across $\{\beta, \kappa, \gamma, \nu_1, \nu_2, \sigma_1, \sigma_2, r, \alpha, \omega\}$. (i) R_e is computed for each draw and (ii) we computed 12-month cumulative cases under only vaccination ($r = \alpha = 0$), only covering ($\nu_1 = \nu_2 = 0$), and both. PRCCs summarizes the global drivers.

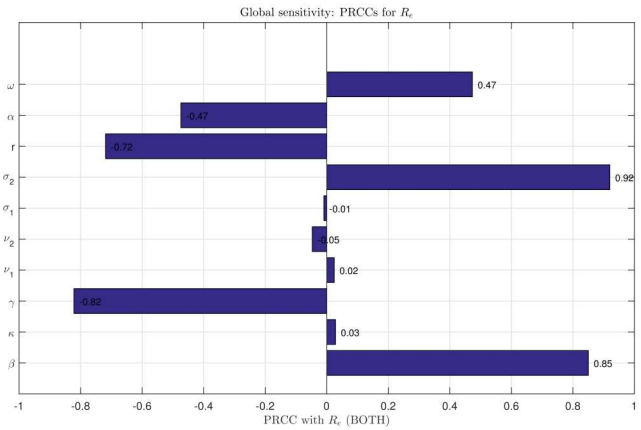

Figure 17: Global sensitivity of R_e (PRCC, "Both" baseline). Positive bars increase R_e; negative bars decrease it. The strongest inflators of R_e are transmission β and residual susceptibility after two doses σ_2; the strongest reducers are recovery γ and the covering effectiveness parameter r. Moderate increase from reversion ω indicates that sustaining covering matters.

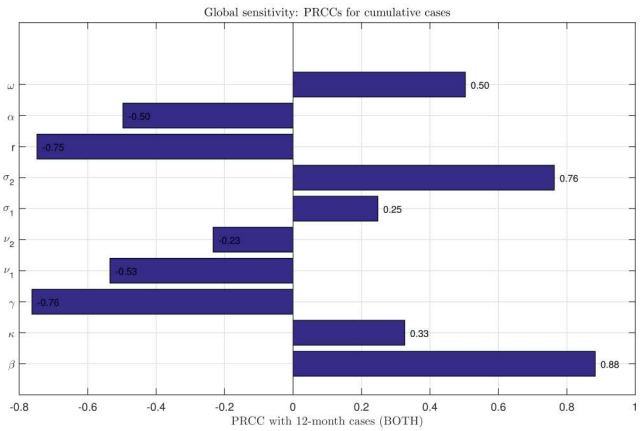

Figure 18: GS of 12-month cumulative cases. Cases increase with β, σ_2, κ, and ω; and decrease with γ, ν_1, and r. α is protective, while ν_2's protective impact is small.

Figure 19 shows the LHS distributions of R_e by regime. We estimate $\Pr(R_e < 1) = 0.243$ under Vaccination-only, 0.000 under Covering-only, and 0.476 under Both. Thus, combining vaccination with covering nearly doubles the chance of immediate control relative to vaccination alone.

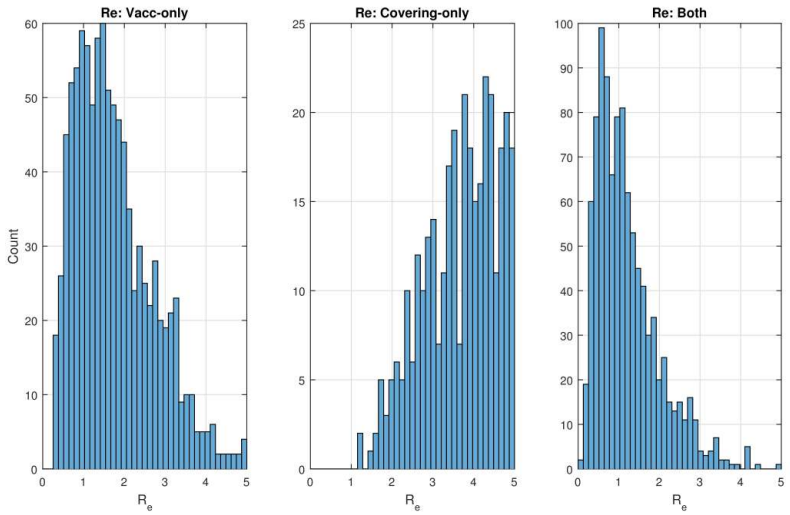

Figure 19: Uncertainty in R_e by regime (LHS histograms). Left: vaccination-only; middle: covering-only; right: both. Mass shifts leftward (toward $R_e < 1$) when vaccination and covering act together; covering alone rarely achieves control.

Twelve-month cumulative cases (Fig. 20) are lowest and most concentrated near the origin when both levers are used, while covering alone performs worst (heavy right tail). Vaccination alone achieves intermediate reductions but leaves substantial probability mass at large outbreak sizes.

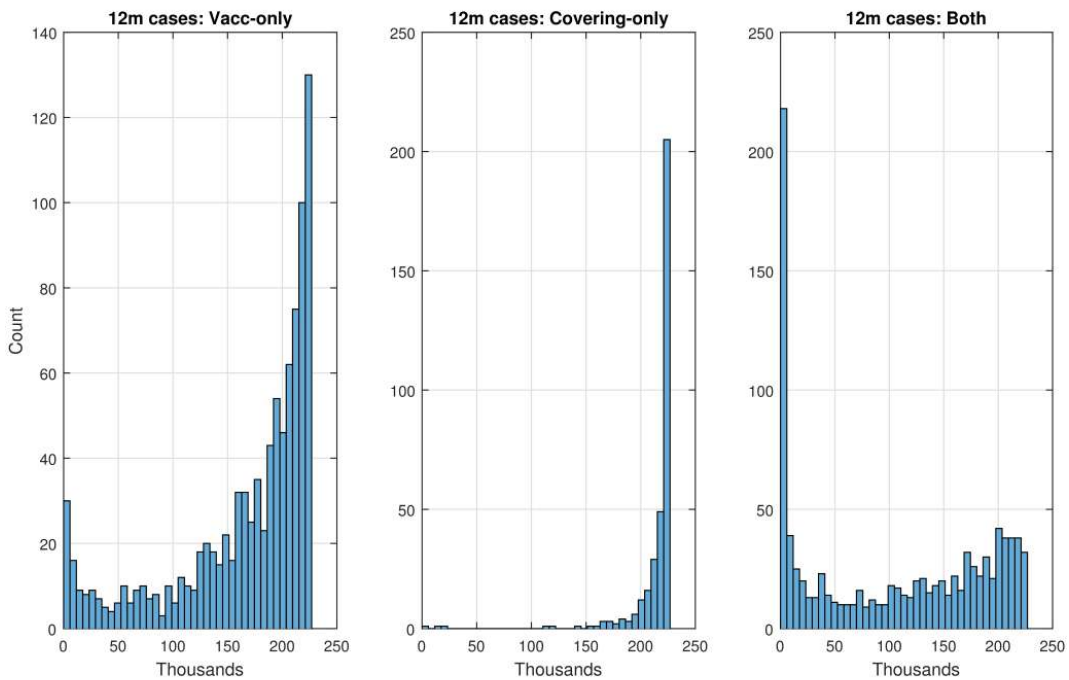

Figure 20: **Uncertainty in 12-month cumulative cases by regime (LHS histograms).** Left: vaccination-only; middle: covering-only; right: both. The combined strategy shifts the whole distribution farthest left, indicating the most robust burden reduction across parameter uncertainty.

Thus, (1) β, γ, r, and σ_2 are the dominant global drivers, targeting contact risk, improving recovery, strengthening covering effectiveness, and maintaining high two-dose protection yield the largest gains. Sustaining behavior (lower ω) is important: loss of covering erodes control even when adoption is adequate. Result reveals that vaccination and covering are complementary under uncertainty; together they nearly double $\Pr(R_e < 1)$ compared with vaccination alone and shift the 12-month burden distribution markedly left.

4.8. Results

We evaluated headline outcomes across four policy regimes using our fitted national model ($R^2 = 0.9688$; see Figure 2). Local one-at-a-time (OAT) sensitivity analyses (Figures 15, 16; Table 2) show that transmission (β), recovery (γ), covering protection (r), and two-dose vaccine effectiveness (σ_2) are the most influential levers on both R_e and case totals. Global sensitivity results using PRCC (Figures 17, 18) confirm these drivers, while also showing the importance of sustaining behavior (low ω).

Uncertainty analyses further clarify regime performance. Twelve-month effective reproduction numbers R_e (Figure 19) show that vaccination-only achieves $P(R_e < 1) = 0.243$, covering-only yields zero chance of control, and combining both levers nearly doubles the chance of suppression (0.476). Distributions of 12-month cumulative cases (Figure 20) are most favorable under the combined regime, intermediate under vaccination-only, and worst under covering-only.

Table 3 distills these outcomes into totals over 1,100 days, illustrating that vaccination alone reduces cumulative cases by 34.2%, covering alone by just 0.2%, while combining both reduces cases by 80.0% and nearly doubles the probability of epidemic control compared with vaccination-only.

Regime	**Cumulative cases (1,100 d)**	$\mathbf{P(R_e < 1)}$
None (baseline fit)	228,275	—
Vaccination-only	150,182 (−34.2%)	0.243
Covering-only	227,908 (−0.2%)	0.000
Both (vaccination+cover)	45,727 (−80.0%)	0.476

Table 3: Scenario totals and control probabilities. Reductions in parentheses are relative to the baseline. (Model fit to national data: $R^2 = 0.9688$; see Figure 2.) $P(R_e < 1)$ are empirical frequencies from the PRCC/LHS runs (Figure 19).

Finally, behavioral persistence emerges as critical. Heatmaps over adoption (α) and protection strength (r) at three levels of reversion ($\omega = 0, 0.05, 0.20$) show that covering only reduces burden when adoption is high and sustained (low ω); otherwise its effect vanishes.

Taken together, these results demonstrate: (1) vaccination and covering are complementary, (2) synergy between them drives the largest gains in epidemic control, and (3) the system's dominant levers are β, γ, r, and σ_2, with behavior persistence (low ω) reinforcing their impact.

5. Conclusion

We set out to close a critical knowledge gap on how biomedical and behavioral interventions work together to influence mpox outbreak control. Although vaccination scale-up has dominated recent policy efforts, the contribution of lesion covering, a low-cost, immediately deployable behavioral measure, has remained largely unquantified. To address this, we constructed a quantitative modelling framework that integrates vaccination throughput with covering practices to evaluate their combined effects on transmission and case burden in the United States, as well as the stability of these effects under uncertainty in biological and behavioral parameters.

The results demonstrate that vaccination and lesion covering work in tandem rather than serving as direct substitutes. Delivering vaccines on their own cut the overall number of cases by about one-third (–34.2%), whereas implementing covering alone produced only a slight change (–0.2%). In combination, however, the two interventions reduced cumulative infections by 80.0% and nearly doubled the probability of driving the effective reproduction number below one, from 0.243 with vaccination only to 0.476 when

both were applied. Yet, covering adoption, added with vaccination, decreases outbreak potential. Our analysis also indicates that covering can slow transmission prior to the full rollout of vaccines, effectively extending the window for immunization efforts to take hold. This benefit, however, is highly sensitive to the persistence of the practice: rapid decline in use ($\omega = 0.20$) removes the advantage, whereas continued adherence ($\omega = 0$) substantially boosts vaccination impact. These patterns highlight that sustaining behavioral engagement is just as crucial as initiating it.

Sensitivity analyses, both local and global, identify transmission rate (β), recovery rate (γ), covering protection strength (r), and two-dose vaccine efficacy (σ_2) as the parameters with the greatest influence on epidemic outcomes. Interventions that speed recovery through faster diagnosis and treatment, extend the durability of two-dose protection, and strengthen or prolong covering behavior substantially reduce both R_e and total cases. For example, a 5% rise in recovery rate lowers R_e by nearly the same proportion and cuts case counts by over 15%. Analysis using Latin Hypercube sampling indicates that implementing covering on its own is insufficient to bring the outbreak under control ($P(R_e < 1) = 0$) and vaccination alone succeeds in just 24.3% of simulations, while adding covering raises that probability to 47.6% and shifts the overall burden distribution towards smaller outbreaks. Such robustness across uncertainty scenarios strengthens the argument for jointly implementing these measures.

Thus, covering serves as a multiplier for vaccination rather than a stand-alone fix. This synergy is particularly valuable where vaccine supply or uptake is constrained. Even relatively brief, moderately scaled campaigns that combine biomedical and behavioral levers achieve far greater reductions in disease burden than single-strategy efforts. These insights highlight the importance of designing response plans that intentionally integrate both forms of intervention. Messaging that encourages lesion covering should be embedded within outbreak control policies rather than treated as peripheral, while ensuring high vaccine effectiveness and rapid delivery remains essential. Sustained adherence to covering, together with preserved vaccine durability, can meaningfully increase the likelihood of epidemic control and minimize cumulative impact.

References

1. Addai, Emmanuel, Mercy Ngungu, Musibau Abayomi Omoloye, and Edmore Marinda. "Modelling the impact of vaccination and environmental transmission on the dynamics of monkeypox virus under Caputo operator." Math. Biosci. Eng 20 (2023): 10174-10199.

2. Agbata, Benedict Celestine, Erjola Cenaj, Raimonda Dervishi, Yahaya Jibrin Danjuma, Mshuur Mary-Anne Shior, Emmanuel Abah, Joseph Solomon Onuche, and Homan Emadifar. "Fractional-order mathematical model for Monkeypox transmission dynamics using the Atangana-Baleanu Caputo operator." BMC Infectious Diseases 25, no. 1 (2025): 1000.

3. Ajmal, Hamda, Elizabeth Hunter, Jim Duggan, Catherine Timoney, and Cathal Walsh. "Agent-based modelling of mpox infection dynamics: simulating disease transmission and control strategies." Journal of Artificial Societies and Social Simulation 27, no. 2 (2024).

4. Awoke, Temesgen D., Semu M. Kassa, Yibeltal A. Terefe, and Manalebish D. Asfaw. "Modeling on cost-effectiveness of monkeypox disease control strategies with consideration of environmental transmission effects in the presence of vaccination." Modeling Earth Systems and Environment 10, no. 5 (2024): 6105-6132.

5. Batiha, Iqbal M., Ahmad A. Abubaker, Iqbal H. Jebril, Suha B. Al-Shaikh, Khaled Matarneh, and Manal Almuzini. "A mathematical study on a fractional-order SEIR Mpox model: analysis and vaccination influence." Algorithms 16, no. 9 (2023): 418.

6. Brainard, Julii, Iain Lake, and Paul R. Hunter. "Evaluation of three control strategies to limit mpox outbreaks in an agent based model." medRxiv (2024): 2024-02.

7. Centers for Disease Control and Prevention (CDC). *2022–2024 U.S. Monkeypox (mpox) outbreak data*. Available at: https://www.cdc.gov/mpox/. Accessed 2024.

8. Centers for Disease Control and Prevention (CDC), National Center for Health Statistics. *Mortality in the United States, 2022. NCHS Data Brief, No. 492*, August 2024. Available at: https://www.cdc.gov/nchs/products/databriefs/db492.htm#:~:text=Life%20expectancy%20estimates%2C%20age%2Dadjusted,cause%2C%20National%20Vital%20Statistics%20System.

9. Centers for Disease Control and Prevention (CDC). *JYNNEOS Vaccination Coverage Among Persons at Risk for Mpox — United States, May 22, 2022–January 31, 2023. MMWR Morbidity and Mortality Weekly Report, Vol. 72, No. 13*, March 31, 2023. Available at: https://www.cdc.gov/mmwr/volumes/72/wr/mm7213a4.htm.

10. Center for Outbreak Response Innovation (CORI). *Mpox: Current Outbreak Summary and Risk Assessment Information*, February 6, 2025. Available at: https://cori.centerforhealthsecurity.org/mpox-0.

11. Centers for Disease Control and Prevention (CDC). *Caring for People with Mpox*, 2023. Available at: https://www.cdc.gov/mpox/caring/index.html#:~:text=others%20such%20as:-,Use%20gauze%20or%20bandages%20to%20cover%20the%20rash%20to%20limit,This%20allows%20them%20to:.

12. De Jong, Maarten, Francesca Calà Campana, Pengfei Li, Qiuwei Pan, and Giulia Giordano. "A novel viral infection model to guide optimal mpox treatment." IEEE Control Systems Letters 7 (2023): 3145-3150.

13. Elemuwa, Christopher Ononiwu, Morufu Olalekan Raimi, Muyi Ainu, Teddy Charles Adias, Rotifa Stella Ufuoma, Uchenna Geraldine Elemuwa, Okechukwu Christian Oginifolunnia, Barbara A. Rath, and Patrick E. Obermeier. "Conquering mpox: A comprehensive public health strategy for addressing mpox and poxvirus infections in nigeria–understanding global trends, transmission dynamics, and effective prevention and control measures in nigeria." JMIR Preprints 14, no. 10 (2024): 2024.

14. Idisi, Isaiah Oke, Kayode Oshinubi, Tunde T. Yusuf, and Adejimi Adeniji. "Comparative Cost-Effectiveness Analysis of Awareness and Treatment Strategies for Controlling Mpox in Diverse Epidemiological Settings." (2025).

15. Jin, Shihui, Tong Guan, Akira Endo, Gregory Gan, A. Janhavi, Gang Hu, Keisuke Ejima, Jue Tao Lim, and Borame L. Dickens. "Effectiveness of different border control strategies for reducing mpox importation risk: a modelling study." The Lancet Regional Health-Southeast Asia 35 (2025).

16. Kuehn, Rebecca, Tilly Fox, Gordon Guyatt, Vittoria Lutje, and Susan Gould. "Infection prevention and control measures to reduce the transmission of mpox: a systematic review." PLOS global public health 4, no. 1 (2024): e0002731.

17. Kubra, Khadija Tul, Samra Gulshan, and Rooh Ali. "Analysis of monkey pox transmission dynamics in society with control strategies under Caputo-fabrizio fractal-fractional derivative." MODELLING IN FRACTIONAL-ORDER SYSTEMS WITH APPLICATIONS IN ENGINEERING (2023): 83.

18. L.N. Nkamba, T.T. Manga, Stability and optimal control of a mathematical model of tuberculosis/AIDS co-infection with vaccination, *Journal of Biological Dynamics*, 13(1), (2021)

19. Mohammed, Mohammed Ibrahim, Michael Adu Ayeh, Vivian Owusu Yeboah, Mark Owusu Kakra, and Atampugre John-Bosco. "The Economic Impact Analysis of Monkeypox Stigma-Related Treatment Delays on Healthcare Systems in West African Communities." Ghana Journal of Nursing and Midwifery 1, no. 4 (2024): 171-197.

20. Michaud, J. *The Current International Mpox Emergency and the U.S. Role: An Explainer*, Kaiser Family Foundation, September 26, 2024. Available at: https://www.kff.org/global-health-policy/issue-brief/the-current-international-mpox-emergency-and-the-u-s-role-an-explainer/.

21. Milwid, Rachael M., Michael Li, Aamir Fazil, Mathieu Maheu-Giroux, Carla M. Doyle, Yiqing Xia, Joseph Cox et al. "Exploring the dynamics of the 2022 mpox outbreak in Canada." Journal of Medical Virology 95, no. 12 (2023): e29256.

22. Mathivanan, Tamilarasi, Radhakrishnan Bheeman, Prasantha Bharathi Dhandapani, Ibrahim Alraddadi, Hijaz Ahmad, and Taha Radwan. "Monkeypox: A New Mathematical Model Using the Caputo-Fabrizio Fractional Derivative." Fractals 2025 (2025): 2540128.

23. Molla, Jeta, Idriss Sekkak, Ariel Mundo Ortiz, Iain Moyles, and Bouchra Nasri. "Mathematical modeling of mpox: A scoping review." One Health 16 (2023): 100540.

24. Naandam, Samuel M., Paul Chataa, Christopher Nikingbong, and Agnes Adom-Konadu. "Optimal control and cost-effectiveness analysis of mitigation strategies for monkeypox virus infection in the presence of routine interventions." medRxiv (2025): 2025-01.

25. Paparini, Sara, Isabelle Whelan, Chikondi Mwendera, Rosalie Hayes, Ismael Maatouk, Rosamund Lewis, Mateo Prochazka Nunez, Antons Mozalevskis, Teodora Wi, and Chloe Orkin. "Prevention of sexual transmission of mpox: a systematic review and qualitative evidence synthesis of approaches." Infectious Diseases 56, no. 8 (2024): 589-605.

26. Ramzan, Sehrish, Syeda Alishwa Zanib, Muzamil Abbas Shah, Nadeem Abbas, and Wasfi Shatanawi. "Analytical study of a modified monkeypox virus model using Caputo–Fabrizio fractional derivatives." Modeling Earth Systems and Environment 10, no. 5 (2024): 6475-6492.

27. Rashid, Saima, Abdul Bariq, Ilyas Ali, Sobia Sultana, Ayesha Siddiqa, and Sayed K. Elagan. "Dynamic analysis and optimal control of a hybrid fractional monkeypox disease model in terms of external factors." Scientific Reports 15, no. 1 (2025): 2944.

28. Rizk, Youssef, Giuseppe Lippi, Brandon M. Henry, Kin Israel Notarte, and John G. Rizk. "Update on Mpox management: epidemiology, vaccines and therapeutics, and regulatory changes." Drugs 85, no. 1 (2025): 1-9.

29. Shen, Mingwang, Hao Lai, and Lei Zhang. "Targeted interventions for individuals at high risk is essential for mpox control." The Lancet Infectious Diseases 24, no. 1 (2024): 8-9.

30. Venkatesh, A., M. Manivel, K. Arunkumar, M. Prakash Raj, Shyamsunder, and S. D. Purohit. "A fractional mathematical model for vaccinated humans with the impairment of Monkeypox transmission." The European Physical Journal Special Topics (2024): 1-21.

31. Zhang, Xu-Sheng, Siwaporn Niyomsri, Sema Mandal, Hamish Mohammed, Miranda Mindlin, Bennet Dugbazah, Solomon Adjei et al. "Cost-effectiveness of vaccination strategies to control future mpox outbreaks in England: a modelling study." The Lancet Regional Health–Europe (2025).

A. Optimal Control Model Formulation

A.1. Baseline (Uncontrolled) Dynamics

For reference, the fitted baseline model is

$$\frac{dS}{dt} = \Lambda - \lambda S - \nu_1 S - \mu S, \tag{A.1}$$

$$\frac{dV_1}{dt} = \nu_1 S - \sigma_1 \lambda V_1 - \nu_2 V_1 - \mu V_1, \tag{A.2}$$

$$\frac{dV_2}{dt} = \nu_2 V_1 - \sigma_2 \lambda V_2 - \mu V_2, \tag{A.3}$$

$$\frac{dE}{dt} = \lambda S + \sigma_1 \lambda V_1 + \sigma_2 \lambda V_2 - (\kappa + \mu) E, \tag{A.4}$$

$$\frac{dI}{dt} = (1-\phi)\kappa E + \omega C - (\alpha + \gamma + \mu + d_I) I, \tag{A.5}$$

$$\frac{dC}{dt} = \phi \kappa E + \alpha I - (\omega + \gamma + \mu + d_C) C, \tag{A.6}$$

$$\frac{dR}{dt} = \gamma (I + C) - \mu R. \tag{A.7}$$

The force of infection and population size are

$$\lambda(t) = \frac{\beta}{N(t)} \big(I(t) + (1 - r_0) C(t) \big), \qquad N(t) = S + V_1 + V_2 + E + I + C + R. \tag{A.8}$$

We introduce two bounded, time-varying policy inputs (controls) on the horizon $[0, T]$:

$$u_v(t) \in [0,1] \quad \text{(vaccination intensity)}, \qquad u_c(t) \in [0,1] \quad \text{(covering support)}.$$

They modulate the baseline rates as follows:

$$\nu_1(t) = \nu_1^{\max} u_v(t), \qquad \nu_2(t) = \nu_2^{\max} u_v(t), \tag{A.9}$$

$$\alpha(t) = \alpha_0 + \big(\alpha_{\max} - \alpha_0 \big) u_c(t), \qquad \omega(t) = \omega_0 - \big(\omega_0 - \omega_{\min} \big) u_c(t). \tag{A.10}$$

where $u_v(t)$ is the fraction of feasible vaccination throughput deployed at time t (0 = no additional push; 1 = maximum achievable capacity). Accordingly, $\nu_1(t)$ and $\nu_2(t)$ are scaled by the capacity bounds $\nu_1^{\max}, \nu_2^{\max}$ and the effort level $u_v(t)$. $u_c(t)$ represents the effort invested in promoting adoption and persistence of lesion covering; it increases the adoption rate $\alpha(t)$ from its fitted baseline α_0 toward the best-attainable $\alpha_{\max}$, and decreases the abandonment rate $\omega(t)$ from ω_0 toward the best-attainable $\omega_{\min}$.

A.2. Objective Functional and Control Set

The primary purpose of incorporating control variables is to identify the optimal strategy that reduces the number of exposed and infectious individuals, while factoring in the costs associated with vaccination deployment and reinforcement coverage Hence, the objective function for this optimal control problem is given by

$$J(u_v^*, u_c^*) \;=\; \min_{u_v, u_c \in [0,1]} \int_0^T \Big[A_E\, E(t) + A_I\, I(t) + A_C\, C(t) + \tfrac{1}{2} \big(B_v\, u_v^2(t) + B_c\, u_c^2(t) \big) \Big]\, dt, \tag{A.11}$$

where $A_E, A_I, A_C > 0$ are nonnegative weighting factors that quantify the relative importance of reducing the exposed and infectious populations, and $B_v, B_c > 0$ are penalty parameters reflecting the effort or expense of applying the control measures. The linear expression $A_E E + A_I I + A_C C$ captures the epidemiological burden, while the quadratic contribution $\frac{1}{2}(B_v u_v^2 + B_c u_c^2)$ accounts for intervention costs.

In particular, $\frac{1}{2}B_v u_v^2$ corresponds to the cost of sustaining vaccination intensity $u_v(t)$ over the time horizon $[0,T]$, and $\frac{1}{2}B_c u_c^2$ represents the analogous cost for maintaining covering support $u_c(t)$.

The optimal control pair is then defined as

$$u^*(t) = \big(u_v^*(t),\, u_c^*(t)\big),$$

chosen so that

$$J(u_v^*, u_c^*) \;=\; \min\big\{J(u_v,u_c) : (u_v,u_c) \in \mathcal{U}\big\}, \tag{A.12}$$

with the admissible set of controls $\mathcal{U}$ specified by

$$\mathcal{U} \;=\; \Big\{(u_v,u_c) :\; u_v(t), u_c(t) \text{ are measurable and } 0 \le u_v(t), u_c(t) \le 1,\; t \in [0,T]\Big\}. \tag{A.13}$$

According to Pontryagin's Maximum Principle [18], the optimal solution $\big(u_v^*(t), u_c^*(t)\big)$ must minimize pointwise the Hamiltonian H, subject to the system of state equations (A.1)–(A.7) and the control definitions in (A.9)–(A.10).

The Hamiltonian associated with the control problem is expressed as

$$\begin{aligned}
H = {} & A_E E + A_I I + A_C C + \tfrac{1}{2}\Big(B_v u_v^2 + B_c u_c^2\Big) \\
& + \lambda_S\Big(\Lambda - \lambda S - \nu_1(t) S - \mu S\Big) \\
& + \lambda_{V_1}\Big(\nu_1(t) S - \sigma_1 \lambda V_1 - \nu_2(t) V_1 - \mu V_1\Big) \\
& + \lambda_{V_2}\Big(\nu_2(t) V_1 - \sigma_2 \lambda V_2 - \mu V_2\Big) \\
& + \lambda_E\Big(\lambda S + \sigma_1 \lambda V_1 + \sigma_2 \lambda V_2 - (\kappa + \mu) E\Big) \\
& + \lambda_I\Big((1-\phi)\kappa E + \omega(t) C - (\alpha(t) + \gamma + \mu + d_I) I\Big) \\
& + \lambda_C\Big(\phi \kappa E + \alpha(t) I - (\omega(t) + \gamma + \mu + d_C) C\Big) \\
& + \lambda_R\Big(\gamma(I + C) - \mu R\Big),
\end{aligned} \tag{A.14}$$

where $\lambda_S, \lambda_{V_1}, \lambda_{V_2}, \lambda_E, \lambda_I, \lambda_C, \lambda_R$ denote the adjoint variables associated with the state variables S, V_1, V_2, E, I, C, R respectively.

By Pontryagin's Maximum Principle, the optimal control problem (A.12) subject to the controlled dynamics (A.1)–(A.7) and the admissible set $\mathcal{U}$ in (A.13) reduces to minimizing the Hamiltonian (A.14) pointwise with respect to (u_v, u_c).

Theorem. Suppose that the control pair (u_v^*, u_c^*) minimizes the objective functional (A.11) subject to the controlled state system (A.1)–(A.7). Then the adjoint variables $\lambda_S, \lambda_{V_1}, \lambda_{V_2}, \lambda_E, \lambda_I, \lambda_C, \lambda_R$ satisfy the following system of differential equations:

$$\frac{d\lambda_S}{dt} = \lambda_S\big(\lambda + \nu_1(t) + \mu\big) - \lambda_E\lambda - \lambda_{V_1}\nu_1(t), \tag{A.15}$$

$$\frac{d\lambda_{V_1}}{dt} = \lambda_{V_1}\big(\sigma_1\lambda + \nu_2(t) + \mu\big) - \lambda_E\sigma_1\lambda - \lambda_{V_2}\nu_2(t), \tag{A.16}$$

$$\frac{d\lambda_{V_2}}{dt} = \lambda_{V_2}\big(\sigma_2\lambda + \mu\big) - \lambda_E\sigma_2\lambda, \tag{A.17}$$

$$\frac{d\lambda_E}{dt} = \lambda_E(\kappa + \mu) - \lambda_I(1-\phi)\kappa - \lambda_C\phi\kappa - A_E, \tag{A.18}$$

$$\frac{d\lambda_I}{dt} = \lambda_I(\alpha(t) + \gamma + \mu + d_I) - \lambda_C\alpha(t) - \lambda_R\gamma - A_I, \tag{A.19}$$

$$\frac{d\lambda_C}{dt} = \lambda_C(\omega(t) + \gamma + \mu + d_C) - \lambda_I\omega(t) - \lambda_R\gamma - A_C, \tag{A.20}$$

$$\frac{d\lambda_R}{dt} = \mu\lambda_R. \tag{A.21}$$

The terminal conditions are

$$\lambda_S(T) = \lambda_{V_1}(T) = \lambda_{V_2}(T) = \lambda_E(T) = \lambda_I(T) = \lambda_C(T) = \lambda_R(T) = 0. \tag{A.22}$$

Furthermore, the optimal control pair $(u_v^*(t), u_c^*(t))$ is expressed as

$$u_v^*(t) = \max\left\{0,\ \min\left\{1,\ \frac{\nu_1^{\max}S(t)\big(\lambda_{V_1} - \lambda_S\big) + \nu_2^{\max}V_1(t)\big(\lambda_{V_2} - \lambda_{V_1}\big)}{B_v}\right\}\right\}, \tag{A.23}$$

$$u_c^*(t) = \max\left\{0,\ \min\left\{1,\ \frac{I(t)(\lambda_I - \lambda_C)(\alpha_{\max} - \alpha_0) + C(t)(\lambda_C - \lambda_I)(\omega_0 - \omega_{\min})}{B_c}\right\}\right\}. \tag{A.24}$$

Proof. Differentiating the Hamiltonian (A.14) with respect to each control variable gives the optimality conditions

$$\frac{\partial H}{\partial u_v} = B_v u_v(t) - \Big[\nu_1^{\max}S(t)(\lambda_{V_1} - \lambda_S) + \nu_2^{\max}V_1(t)(\lambda_{V_2} - \lambda_{V_1})\Big] = 0, \tag{A.25}$$

$$\frac{\partial H}{\partial u_c} = B_c u_c(t) - \Big[(\alpha_{\max} - \alpha_0)I(t)(\lambda_I - \lambda_C) + (\omega_0 - \omega_{\min})C(t)(\lambda_C - \lambda_I)\Big] = 0. \tag{A.26}$$

Solving the optimality conditions (A.25)–(A.26) yields the explicit control characterizations (A.23)–(A.24). Since the admissible set of controls $\mathcal{U}$ requires $0 \le u_v(t), u_c(t) \le 1$ for $t \in [0, T]$, the controls are projected onto $[0, 1]$ using the standard $\max\{0, \min\{1, \cdot\}\}$ operator.

S. Jain,
Department of Mathematics,
Poornima College of Engineering, Jaipur 302022,
India.
E-mail address: shilpijain1310@gmail.com

and

T. S. Faniran,
F.I. Proctor Foundation,
University of California, San Francisco, USA
Lead City University, Ibadan, Nigeria.
E-mail address: Taye.Faniran@ucsf.edu

and

M. O. Adewole,
School of Mathematical Sciences,
Universiti Sains Malaysia, Malaysia
Department of Computer Science and Mathematics,
Mountain Top University, Prayer City, Ogun State, Nigeria.
E-mail address: olamatthews@ymail.com

and

L. N. Nkamba,
University of Yaounde I, Yaounde, Cameroon.
E-mail address: lnkague@gmail.com

and

P. Agarwal,
Department of Mathematical Sciences,
Saveetha School of Engineering, Chennai, Tamilnadu, 602105, India
Department of Mathematics,
Anand International College of Engineering,
Jaipur-303012, Rajasthan, India.
E-mail address: goyal.praveen2011@gmail.com

and

H. Jafari,
Department of Mathematical Sciences,
University of South Africa, UNISA0003,
South Africa.
E-mail address: Jafari.usern@gmail.com